3 Experimental details

This chapter describes the details about the synthesis of nanoadditives and the formulation of greases. Brief procedures adopted to assess the physicochemical and tribological properties of greases are discussed. Further, the characterization techniques used for examining the nanoadditives and worn surfaces are also specified.

3.1 Materials

3.1.1 Base oil

The base oil is the main ingredient of the grease. In the present study, one type of mineral oil (i.e., paraffin oil) and two types of vegetable oils (i.e., castor and coconut oils) have been used as base oils to formulate mineral and vegetable oil–based greases, respectively. Paraffin oil, castor oil, and coconut oil are chosen in this study were of analytical grades and procured from S D Fine Chem Pvt. Ltd., Sisco Research Laboratories Pvt. Ltd Qualikems Fine Chem Pvt. Ltd., respectively. The density of paraffin, castor, and coconut oils at 15 ^{o}C was determined as per the ASTM D 4052 standard. The kinematic viscosity of all oil samples was evaluated at 40 ^{o}C and 100 ^{o}C according to the ASTM D 445 standard. Further, the viscosity index (VI) of all base oils was estimated as per the ASTM D 2270 standard. The summary of the physicochemical properties of paraffin, castor, and coconut oils is listed in **Table 3.1**. The wettability of paraffin, castor, and coconut oils on a polished steel surface was examined by the sessile drop method using a contact angle goniometer (DSA–25, Kruss, Germany). A 20 µL volume of a sessile drop of each oil sample was used to measure the contact angles.

Table 3.1: The physicochemical properties of paraffin, castor, and coconut oils

Base oil	Density (g/cm^3), at 15 ^{o}C	Kinematic viscosity (mm^2/s)		Viscosity index
		40 ^{o}C	100 ^{o}C	
Paraffin	0.854	81.17	9.31	88
Castor	0.946	247.52	19.38	88
Coconut	0.908	27.69	6.00	153

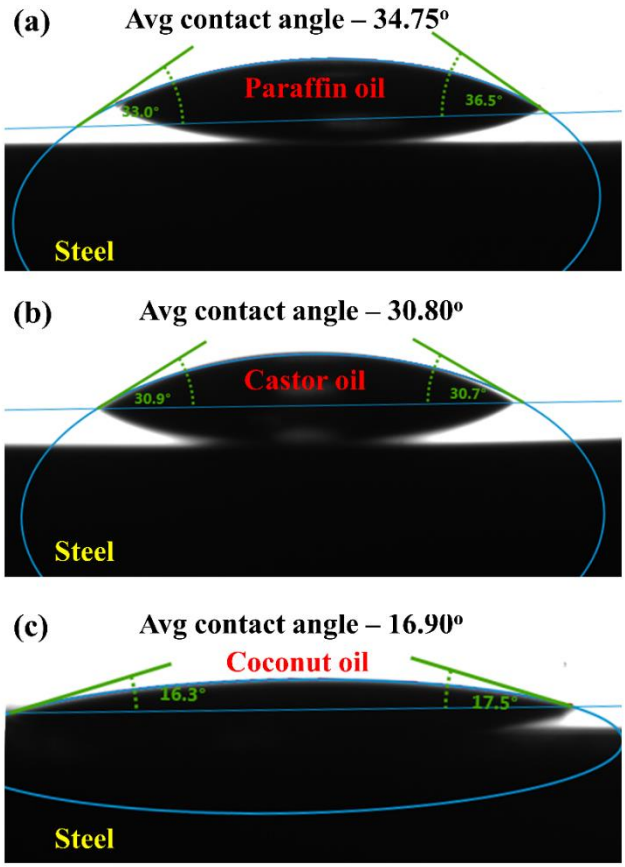

Figure 3.1: Contact angle of (a) paraffin oil, (b) castor oil, and (c) coconut oil on the steel surface

The wettability of lubricating oil on steel surfaces depends on the hydrocarbon chain length and molecular structure of the base oil. It has a significant influence on the lubrication performance of lube oil. If the contact angle of the oil drop with the mating surface is more, it indicates low wettability and vice–versa. Paraffin, castor, and coconut oils were used as a base oil to formulate the grease samples in the present work. **Figure 3.1** displays the

contact angle via sessile drops of paraffin oil, castor oil, and coconut oil on a polished steel plate. The average contact angle furnished by paraffin oil, castor oil, and coconut oil was found to be ~35 deg, ~31 deg, and ~17 deg, respectively. The contact angle formed by coconut oil was less among all base oils; it indicates that coconut oil has superior wettability with a steel surface. Prabhu et al. (2009) have reported the contact angles of mineral oil and coconut oil on the stainless–steel surface and found them to be 28 deg and 19.5 deg, respectively. It suggests that the wettability of vegetable oil is excellent than mineral oil. The excellent wettability of coconut oil could help to enhance the lubrication effect of coconut grease.

3.1.2 Grease thickener

The thickener imparts a unique property to the lubricating oil. In the present study, the lithium soap was formulated via an in–situ saponification reaction between the 12–hydroxystearic acid and lithium hydroxide monohydrate. The 12–hydroxystearic acid and lithium hydroxide monohydrate were procured from Tokyo Chemicals Industry Co. Ltd. and Spectrochem Pvt. Ltd., respectively.

3.1.3 Chemical used in the synthesis of nanoadditives

In the present study, molybdenum disulfide (MoS_2), chemically functionalized molybdenum disulfide with long–chain octadecanethiol (MoS_2–ODT), graphene oxide (GO), reduced graphene oxide (rGO), and chemically functionalized graphene oxide with long–chain octadecylamine (GO–ODA) and silicon dioxide (SiO_2) nanoadditives were synthesized. Therefore, a variety of chemicals were used for the synthesis of these nanoadditives. **Table 3.2** summarized the chemicals being used for the synthesis of nanoadditives.

Table 3.2: List of chemicals used in the synthesis of nanoadditives

Chemical name	Chemical formula	Used for	Assay (%)	Company
Sodium molybdate	$Na_2MoO_4.2H_2O$	Synthesis	99.5	Sigma– Aldrich
Hydroxylamine hydrochloride	$NH_2OH.HCl$	Synthesis	99	Alfa Aesar
Thiourea	NH_2CSNH_2	Synthesis	99	Sigma– Aldrich
Hydrochloric acid	HCl	Synthesis	35	Merck Millipore
Methanol	CH_3OH	Synthesis	99.9	Merck Millipore
Ethanol	C_2H_5OH	Synthesis	99.9	Merck Millipore
1–octadecanethiol	$C_{18}H_{38}S$	Grafting	98	Sigma– Aldrich
Sulfuric acid	H_2SO_4	Synthesis	98	Merck Millipore
Graphite powder (<20µm)	C	Synthesis	—	Sigma Aldrich
Potassium permanganate	$KMnO_4$	Synthesis	99	Fischer Scientific
Sodium nitrate	$NaNO_3$	Synthesis	98	Alfa Aesar
Hydrogen peroxide	H_2O_2	Synthesis	30	Loba Chemie
Hydrazine hydrate	N_2H_2	Synthesis	50–60	Sigma–Aldrich
Octadecylamine	$C_{18}H_{39}N$	Grafting	90	Merck Millipore
Tetraethoxysilane	$C_8H_{20}O_4Si$	Synthesis	>96.0	TCI Chemicals
Ammonia	NH_3	Synthesis	28–30	ACS Reagent

3.2 Synthesis of nanoadditives

3.2.1 Synthesis of MoS_2 and MoS_2–ODT nanosheets

The MoS_2 nanosheets were prepared by a hydrothermal reduction of sodium molybdate with thiourea (Kumari et al., 2017). The flowchart for the synthesis process of MoS_2 nanosheets by the hydrothermal method is shown in **Figure 3.2**. In this context, the aqueous solution (10 mL) of sodium molybdate (0.625 g) and hydroxylamine hydrochloride (0.35 g) was added gradually with a 2.5 mL HCl (35% aqueous solution) under continuous

stirring for 30 min at 90 ^{o}C. A 0.78 g thiourea was then progressively added to the reaction solution and stirred for another 15 min. The reaction precursors of MoS_2 were then charged into Teflon–lined stainless steel autoclave and kept in the conventional hot air oven at 230 °C for 24 h. During the hydrothermal reduction, the solution phase of reaction precursors converted into the segregated black color product of MoS_2. The MoS_2 was centrifuged at 5000 rpm and washed with distilled water for several cycles until the pH of decanted water reached nearly 7. In the final step, the MoS_2 nanosheets were separated by filtration and dried in a conventional hot air oven at 90 ^{o}C. The dried MoS_2 nanosheets were grounded with a mortar and pestle into fine powder for further use and characterization.

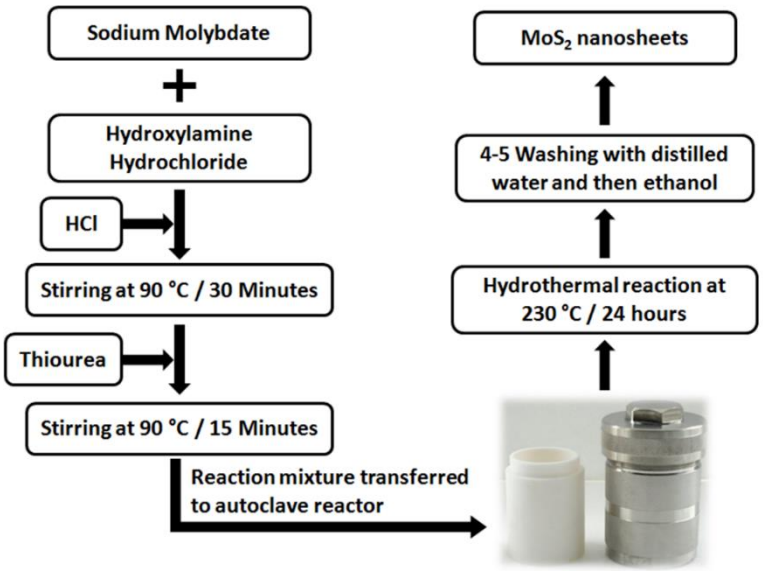

Figure 3.2: Flowchart for the synthesis process of MoS_2 nanosheets by hydrothermal reduction

The cohesive interaction between the dangling sulfur atoms of MoS_2 lamella due to van der Waals forces causes agglomeration of MoS_2 nanosheets. The chemical functionalization of nanoadditives with surface–active molecules is one of the most attractive methods to avoid the agglomeration of nanoadditives. The MoS_2 nanosheets were functionalized via a long alkyl chain. A schematic illustration on the functionalization of MoS_2 nanosheets with ODT

molecules is shown in **Figure 3.3**. In this context, 0.6 g of 1–octadecanethiol (ODT) was added in 50mL methanol to prepare the ODT solution. The MoS_2 nanosheets (0.11 g) were dispersed in ODT solution with the aid of ultrasound energy. The sonication of the reaction mixture was carried out using a bath sonicator. The resultant product was separated via filtration using Teflon membrane and washed with methanol for several cycles to remove the physisorbed traces of ODT. In the last step, the functionalized MoS_2 nanosheets were dried in a conventional hot air oven at 90 ^oC. The dried MoS_2–ODT nanosheets were grounded with a mortar and pestle into fine powder for further use and characterization.

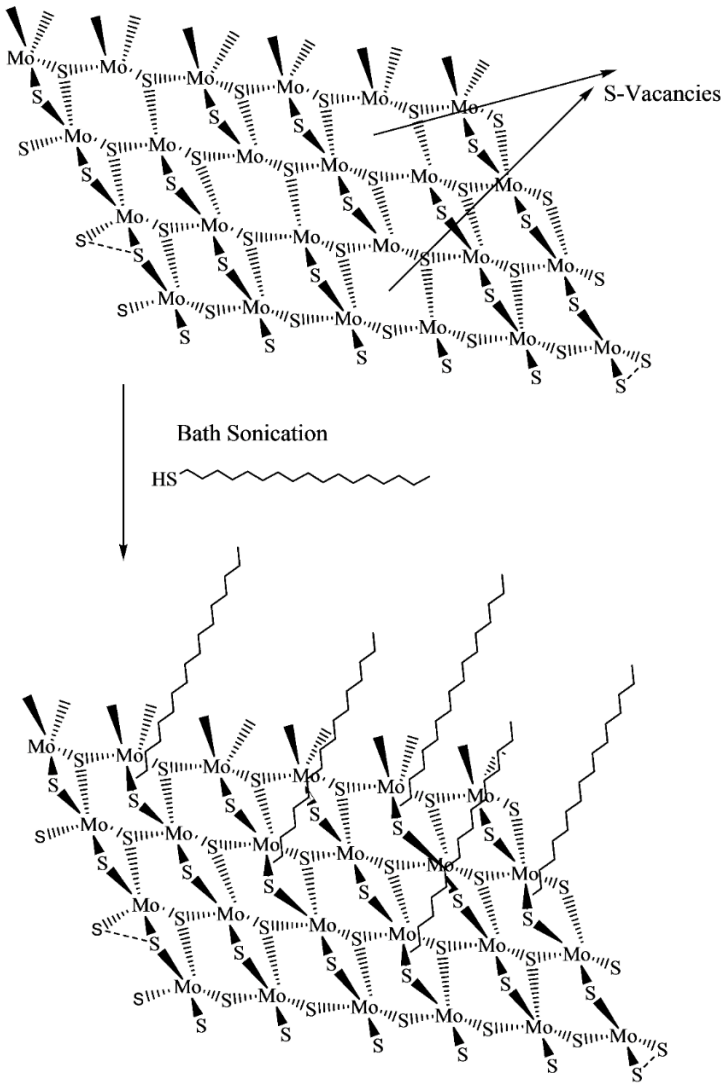

Figure 3.3: A schematic illustration on functionalization of MoS_2 nanosheets with ODT (Kumari et al., 2017)

3.2.2 Synthesis of GO, rGO, and GO–ODA nanosheets

The GO nanosheets were prepared by the Hummers method via severe oxidation, followed by exfoliation of graphite powder (Mungse and Khatri, 2014). In this typical procedure, 5 g graphite flakes (< 20 µm), 5 g $NaNO_3$, and 230 mL of H_2SO_4 were blended in a reaction vessel under continuous stirring in an ice bath. A 30 g $KMnO_4$ was added gradually to the reaction mixture. The reaction mixture was left under continuous stirring for 24 h at room temperature. The $NaNO_3$, H_2SO_4, and $KMnO_4$ are strong oxidizing reagents used to oxidize graphite powder into graphite oxide. After that, 400 mL of distilled water was added gradually to the reaction mixture. Subsequently, the reaction mixture was transferred to an oil bath and continued stirring for 24 h, and the temperature of the reaction vessel was maintained at 98 ^oC. On the next day, 1 L distilled water was added slowly to the reaction mixture. Further, 30% hydrogen peroxide (100 mL) was added into the reaction mixture to stop the oxidative events, followed by a 5% HCl aqueous solution to eliminate the undigested residue of oxidizing reagents. The oxidized graphite was turned into dark brown dispersion, which was rinsed with plenty of distilled water. The pH of decanted water reached nearly 7, which confirmed the elimination of acidic contents. It was followed by the exfoliation of graphite oxide into GO through sonication using an ultrasonic probe. The aqueous solution enriched with highly dispersed GO nanosheets was centrifuged at 5000 rpm for 20 min. The collected supernatant having fine GO nanosheets was dried in a conventional hot air oven at 90 ^oC. The dried GO nanosheets were grounded with a mortar and pestle into fine powder for further use and characterization.

The rGO nanosheets were prepared by chemical reduction using hydrazine hydrate as a reducing reagent. A schematic illustration on the reduction of GO into rGO nanosheets is shown in **Figure 3.4**. In this process, 25 mL of hydrazine hydrate was added into the

aqueous solution dispersion of GO nanosheets and refluxed it for 24 h under continuous stirring at 100 ^{o}C. After completing the chemical reduction process, the rGO was transformed into black color due to eliminating oxygen functionalities. The resulting product was obtained as an aggregated and non–dispersed form at the bottom of the reaction vessel. It was separated by filtration using a 0.2 µm pore size membrane and rinsed with plenty of distilled water (several cycles) to remove the residual traces of hydrazine hydrate. Finally, the black color filtrate wet cake of rGO nanosheets was dried in a conventional hot air oven at 90 ^{o}C. The dried rGO nanosheets were grounded with a mortar and pestle into fine powder for further use and characterization.

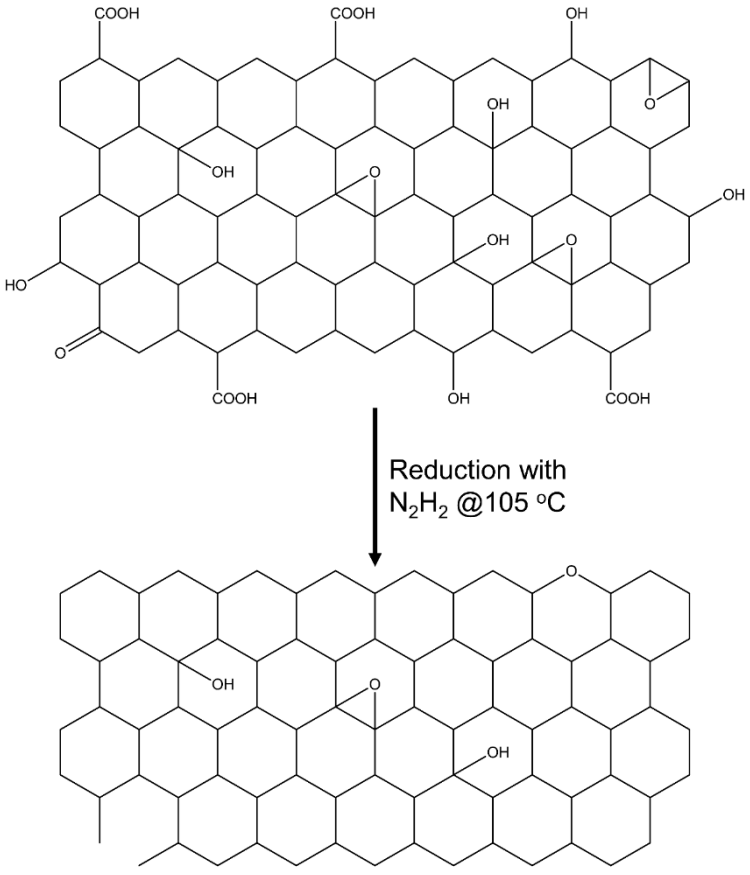

Figure 3.4: A schematic illustration on the reduction of GO into rGO using hydrazine hydrate as reducing agent

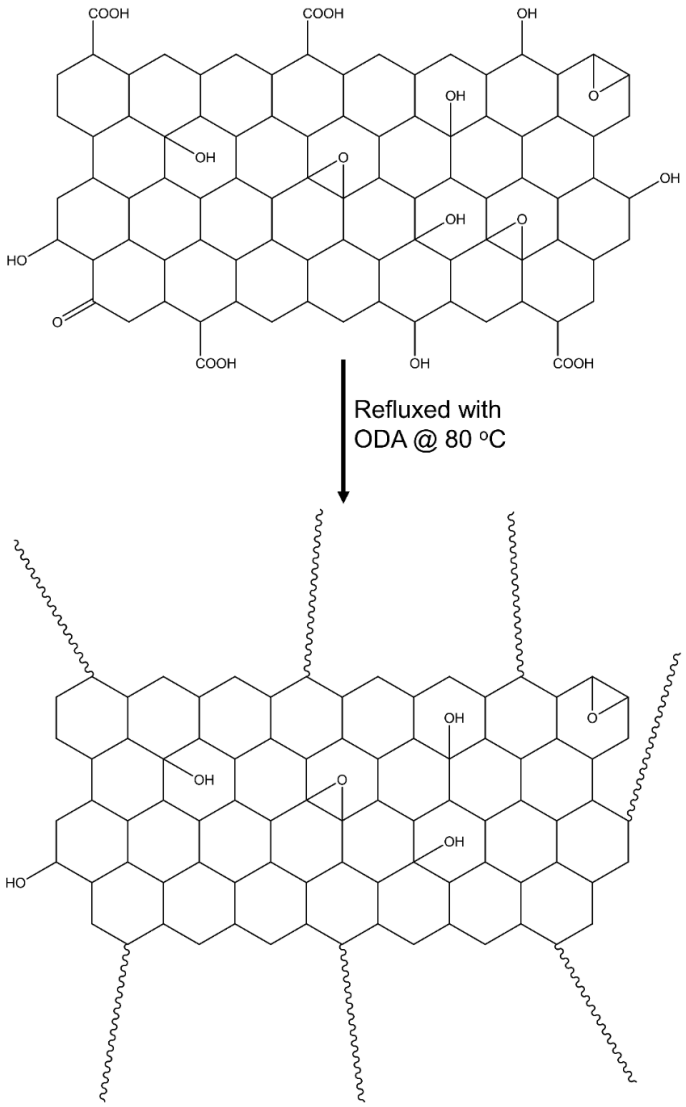

Figure 3.5: A schematic illustration on functionalization of GO nanosheets with ODA molecules

The GO–ODA nanosheets were prepared by chemical functionalization of a long alkyl–chain constituted ODA over the GO. A schematic illustration on the functionalization of GO nanosheets with ODA molecules is shown in **Figure 3.5**. In the first step, 20 g of ODA was dissolved in 125 mL of ethanol to obtain homogenous ethanolic solution of ODA. In the second step, the prepared dispersion was added gradually in the aqueous dispersion of GO nanosheets in a reaction vessel. Subsequently, the reaction mixture was refluxed overnight under continuous stirring, and the temperature was maintained at 80 ^{o}C. The

black color aggregated GO–ODA nanosheets were separated by filtration using a 0.2 µm pore size membrane. The resulting product was rinsed with ethanol several times to remove the excess content of ODA. Finally, the shiny black color filtered cake of GO–ODA nanosheets was dried in a conventional hot air oven at 90 ^{o}C. The dried GO–ODA nanosheets were grounded with a mortar and pestle into fine powder for further use and characterization.

3.2.3 Synthesis of SiO_2 nanoparticles

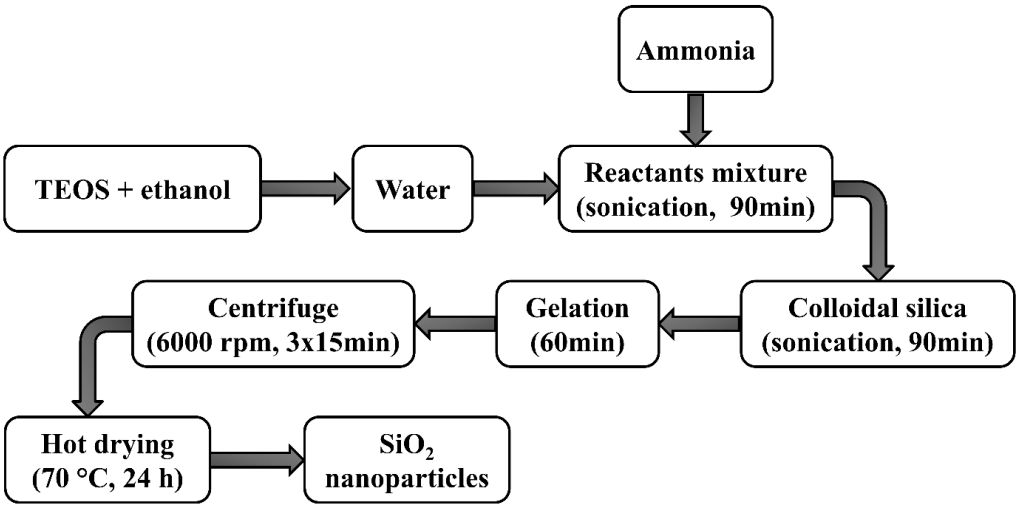

Figure 3.6: Flowchart for synthesis process of SiO_2 nanoparticles by modified sol–gel method

The SiO_2 nanoparticles were synthesized by a modified sol–gel method (Jafarzadeh et al., 2009). The flowchart for the synthesis process of SiO_2 nanoparticles by the modified sol–gel method is shown in **Figure 3.6**. In this synthesis route, 10 mL of TEOS was homogeneously dissolved in 60 mL ethanol using a bath sonicator at room temperature. After that, the reaction mixture was kept in an ice bath, and the temperature was maintained at less than 30 ^{o}C. Subsequently, the 2 mL distilled water was added drop–wise into the reaction solution with the feed rate of 0.2 mL/min for facilitating TEOS hydrolysis through sonication using an ultrasonic probe. After 90 min, the 4 mL aqueous NH_3 was slowly

added into the reaction mixture with the feed rate of 0.05mL/min, and sonication was continued for the next 3 h followed by gelation for the next 1 h. The prepared white color SiO_2 gel was centrifuged at 6000 rpm for 15 min and rinsed the reaction mixture with a blend of ethanol and distilled water (1:1). The washing and centrifugation were repeated until the pH of decanted water reached nearly 7. The SiO_2 gel separated by centrifugation was dried in the conventional oven at 70 °C and grounded with a mortar and pestle into fine powder to obtain the SiO_2 nanoparticles.

3.3 Characterization of nanomaterials

3.3.1 Transmission electron microscope (TEM)

The morphological and nanostructural features of MoS_2, MoS_2–ODT, GO, rGO, GO–ODA, and SiO_2 nanoadditives were examined using a high–resolution transmission electron microscope (TEM), JEM 2100, JEOL Ltd., (Japan). For sample preparation, the ethanolic dispersion of each nanoadditives was drop–casted on a separate TEM grid (copper material, diameter–3 mm, thickness–100 µm, and 200 mesh lacey carbon). The operating voltage was kept constant at 300 kV, and a high vacuum in the range of 10^{-6} Torr is required to acquire the low and high–resolution TEM images.

3.3.2 X–ray diffractometer (XRD) spectroscopy

X–ray electromagnetic are waves of high energy, and their wavelength is shorter than visible light. XRD spectroscopy is the most effective method to probe the crystalline structure and identify the different phases of materials having the same composition. X–ray beams incident on powder or thin film samples will be diffracted because of crystallographic planes. Bragg's Law is the basic principle of diffraction. Bragg's equation

was used to evaluate the interlamellar spacing between parallel successive crystallographic planes.

$$n\lambda = 2d\sin\theta \qquad \text{Eq (3.1)}$$

Where, n is an integer; λ is wavelength of incident X–ray radiation; d is interlamellar spacing between parallel successive crystallographic planes; θ is incident angle.

The crystalline features of MoS_2, MoS_2–ODT, GO, rGO, and GO–ODA was probed by an X–ray diffractometer (XRD), Rigaku Miniflex 600 D/teX Ultra using Cu Kα line as an X–ray radiation source. The wavelength (λ) of the radiation was 0.15418 nm. The typical voltage and current were kept constant at 40 kV and 15 mA, respectively. The XRD patterns of MoS_2, MoS_2–ODT, and SiO_2 samples were collected in the 2θ range of 10 to 80°, whereas the XRD patterns of GO, rGO, and GO–ODA samples were collected in the 2θ range of 2 to 70°.

3.3.3 Fourier transform infrared (FTIR) spectroscopy

FTIR spectroscopy was used to explore the various functional groups present in solid, liquid, and gaseous samples by acquiring an infrared spectrum of absorption or transmittance. The nanoadditives, viz. MoS_2, MoS_2–ODT, SiO_2, GO, rGO, and GO–ODA were individually grounded with KBr (dry) powder to make the pellets and collect their FTIR spectra. The transmittance FTIR spectra of MoS_2, MoS_2–ODT, GO, rGO, and GO–ODA were obtained using Thermo–Scientific Nicolet 8700 spectrometer at a resolution of 4 cm^{-1} in the spectral range between 400 and 4000 cm^{-1}. It was used to affirm the formulation and chemical functionalization of nanoadditives.

3.4 Synthesis of grease

In the present study, the mineral and vegetable oil–based greases were synthesized using paraffin oil, castor oil, and coconut oil as base oil and 12–lithium hydroxystearate metallic soap as a thickener. The grease samples were prepared by in–situ saponification reaction between a 12–hydroxystearic acid and lithium hydroxide monohydrate. The soap concentration was fixed at 14% w/w. Batches of 250 g grease samples were prepared, so it required 35 g of 12–lithium hydroxystearate. Therefore, the detailed calculation of the stoichiometric amount of 12–hydroxystearic acid and lithium hydroxide monohydrate was required to formulate a 250 g sample of grease as presented in **Appendix–A**.

Each nanoadditives sample was individually dispersed into base oil at different concentrations in the range between 0.01–0.05% w/w. A measured quantity of nanoparticles was dispersed into the base oil using a magnetic stirrer (IKA, C–MAG HS4 digital) at room temperature for 30 min. For homogenous dispersion of nanoadditives in the base oil, it was kept in a water bath sonicator (Antech, GT–1730QTS) at room temperature for 1 h. Overhead mechanical stirrer (Remi Elektrotechnik Ltd, 8000 rpm) appended with a square–edged anchor impeller was used to stir the solution. 12–hydroxystearic acid was added slowly into the mixture, stirred continuously at 200±10 rpm, and heated at 90±2 ^{o}C. In parallel, lithium hydroxide monohydrate was dissolved homogeneously in distilled water and added dropwise to the mixture as soon as 12–hydroxystearic acid started to melt, and a waxy transformation occurs. The mixture was allowed to stir at 300±10 rpm at a temperature of 180±2 ^{o}C for 2 h followed by cooling at room temperature for 24 h.

3.5 Characterization of greases

National Lubricating Grease Institute (NLGI), in association with the American Society of Testing Materials (ASTM), has standardized the test specifications and procedures for grease testing. The physicochemical properties (i.e., consistency and drop point) and tribological properties (i.e., AW and load–bearing capacity) of greases were assessed as per ASTM standards.

3.5.1 Characterization of physicochemical properties of greases

The consistency and drop point are essential properties of the greases. The word *consistency* indicates the thinness or thickness related to the flowability of grease. The consistency is primarily controlled through the type and concentration of thickener, but the viscosity of base oil has a minor influence on it. The drop point is also a critical property to evaluate the performance of the grease. When the grease is heated, it softens and turns its phase from semi–solid to liquid.

3.5.1.1 Consistency

In the present study, the consistency of all grease samples was measured using the cone penetrometer (Khusboo Scientific Instrument Pvt. Ltd., India) as per the ASTM D1403 standard. The schematic diagram of the cone penetrometer is shown in **Figure 3.7**. When the quantity of grease sample is limited, the one–half (½) or one–quarter (¼) scale cone equipment is used to determine the consistency of the grease. This test evaluates the unworked and worked penetration depth, which designates the grease's NLGI consistency number. In this test, a standard cone assembly was released to sink freely in the grease for 5 s at 25 ^{o}C. The penetration depth is measured by a dial gauge attached with cone penetration equipment. The unit of measured penetration is in tenths of a millimeter.

The test condition for unworked and worked penetration measurements are the same as described in **Table 3.3**. If the penetration measurements are acquired with ½ scale or ¼ scale, the cone penetrometer must be converted to full scale as per the following equations (ASTM D1403).

For ½ scale,

$$P = 2p' + 5 \qquad \text{Eq (3.2)}$$

Where, P = cone penetration by test method D 217, and

p'= cone penetration by ½ scale equipment

For ¼ scale,

$$P = 3.75p'' + 24 \qquad \text{Eq (3.3)}$$

Where, P = cone penetration by test method D 217, and

p" = cone penetration by ¼ scale equipment

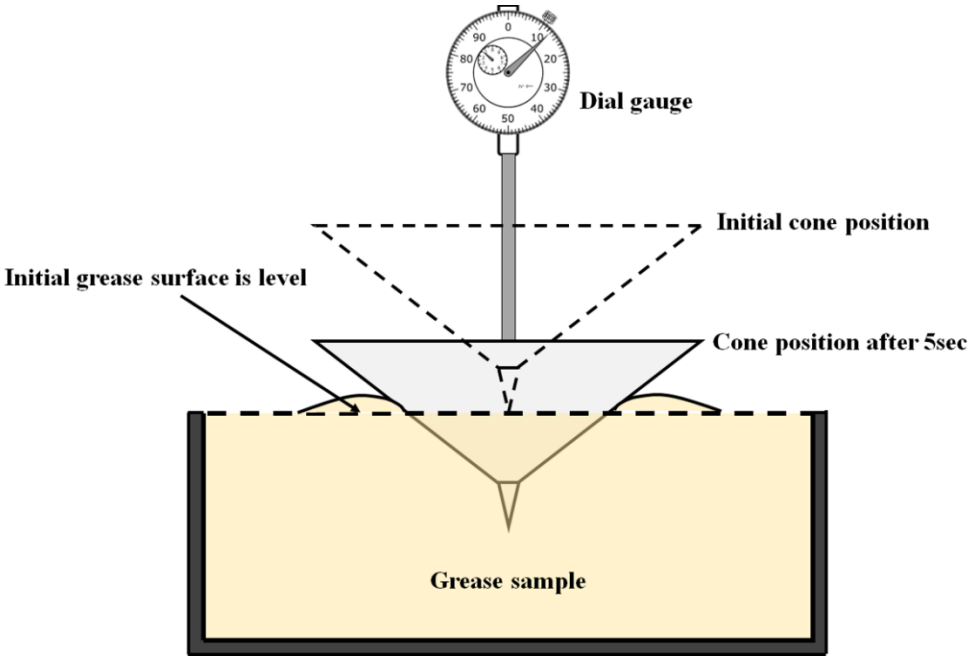

Figure 3.7: The schematic diagram of cone penetration test set–up

Table 3.3: Prescribed test conditions used for determination of the grease consistency (ASTM D217; ASTM D1403)

ASTM Standard	Type of scale	Weight of cone assembly, g	Quantity of grease, g	Duration, s	Temperature, °C
D 217	Full scale	150±0.100	400	5±0.1	25±0.5
D 1403	Half scale	37.5±0.050	—	5±0.1	25±0.5
	Quarter scale	9.38±0.025	—	5±0.1	25±0.5

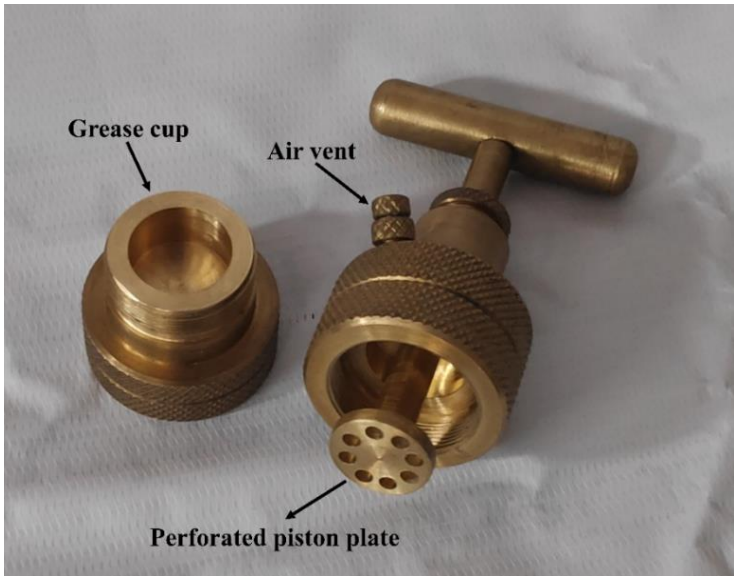

Figure 3.8: The image of ¼ scale grease worker

Table 3.4: Grades of grease classified by NLGI (ASTM D217)

NLGI grade	Work penetration depth after 60 strokes at 25 °C (0.1 mm)	Appearance
000	445–475	Fluid
00	400–430	Semi–fluid
0	355–385	Very soft
1	310–340	Soft
2	265–295	Normal
3	220–250	Firm
4	175–205	Very firm
5	130–160	Hard
6	85–115	Very hard

In unworked penetration, the measurements are obtained on the undisturbed grease structure. In worked penetration, a grease worker is used to shear the grease structure. The image of the ¼ scale grease worker is depicted in **Figure 3.8**. The grease worker has a perforated disc, which shears the grease structure through the holes twice at every grease worker arm stroke. As per the standard 60 strokes, a furnished grease sample was used to measure the worked penetration depth. The mechanical working amends the penetration depth of the grease. The NLGI consistency number designation of the grease is based on worked penetration depth measurements. NLGI consistency number classifies the grease's hardness in the range between 85 (NLGI 6) to 475 (NLGI 000). NLGI 000 attributes to *fluid*, and NLGI 6 ascribes for *hard* grease. The classification system of NLGI is reported in **Table 3.4**.

3.5.1.2 Drop point

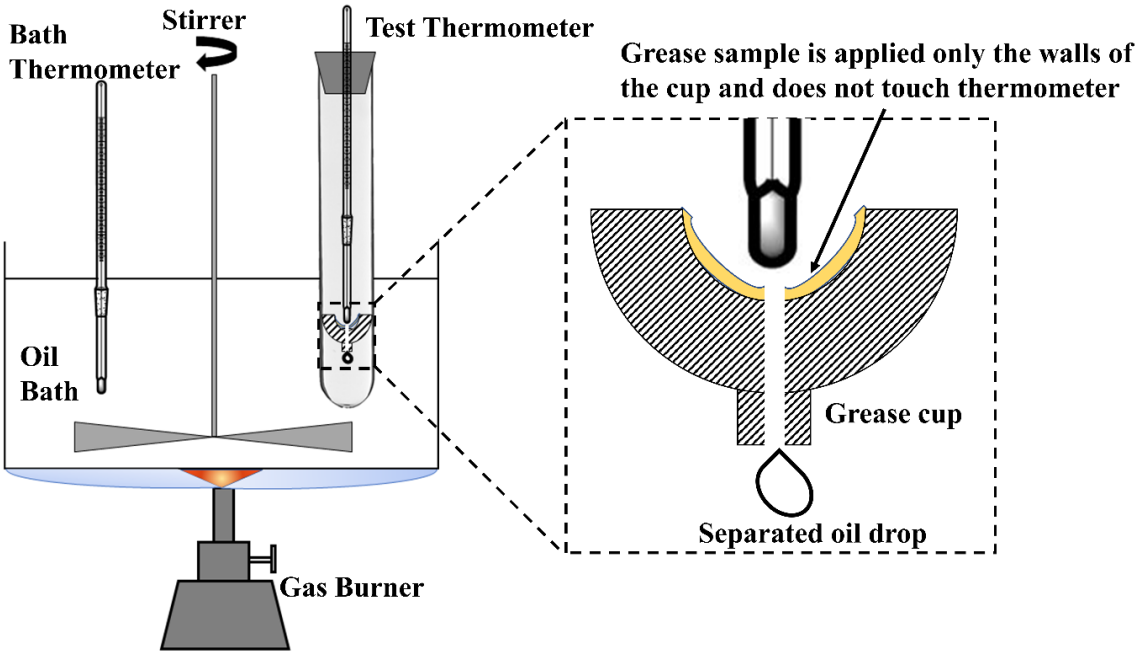

Figure 3.9: The image of drop point equipment

The drop point is another significant characteristic of grease. The drop point is the temperature at which grease transforms its phase from the semi–solid to liquid. The drop point is referred to as the *melting point* of the grease. At this temperature, the thickener faded its property to constrain base oil within its fibrous network. Some non–soap–based grease does not melt with the increment of temperature and can be stable up to either the thickener or base oil's decomposition temperature. Therefore, these greases do not show a drop point and are preferably used for bakery ovens. The drop point of grease samples was evaluated using the drop point apparatus (Khusboo Scientific Instrument Pvt. Ltd., India) as per the ASTM D566 standard. The schematic diagram of the drop point apparatus is shown in **Figure 3.9**.

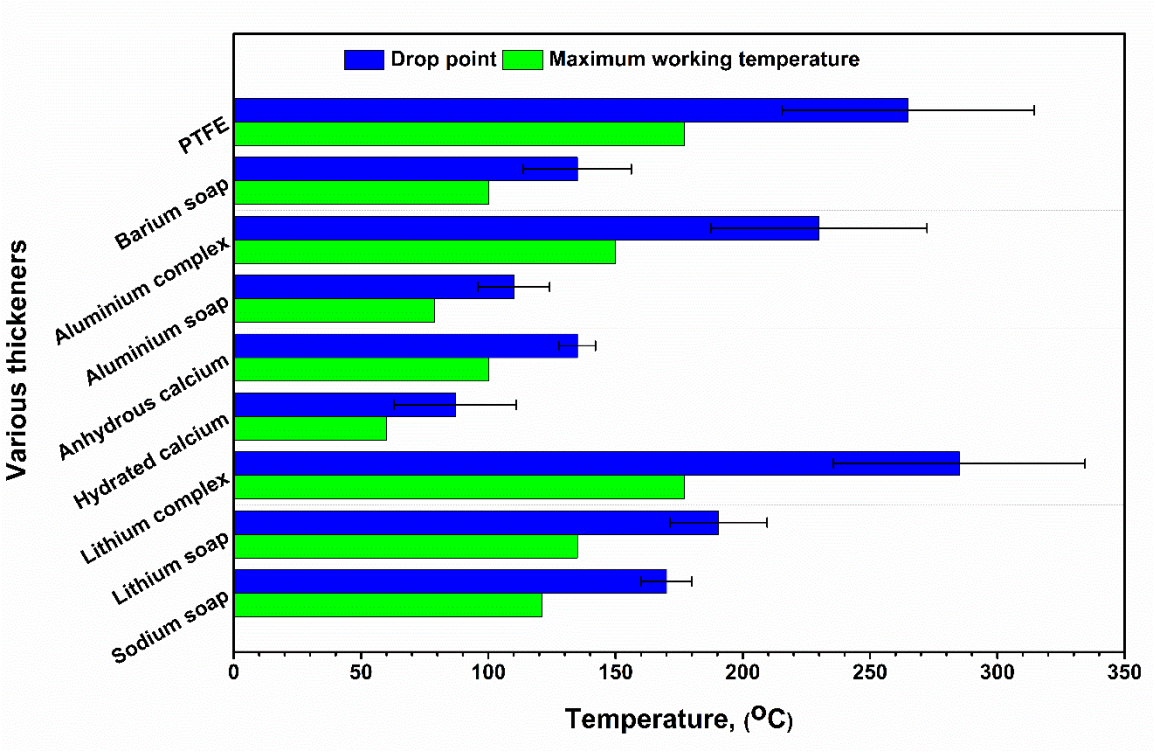

Figure 3.10: Effect of thickener on the drop point of the grease

In this test, the grease was heated under prescribed conditions. When the first drop of oil was detached from the grease matrix and fell in the bottom of the tube, that temperature was referred to as *drop point*, which was an average of two thermometers reading. In this

test method, the bath temperature is limited up to 288 ^{o}C and determined of drop point of grease over the wide range of temperature through ASTM D2265 standard. The thickener used in the grease formulation affects the drop point and the maximum useful working temperature of the grease. The effect of thickener on the drop point of the grease is represented in **Figure 3.10**. The standard deviation indicates the range of variation in the drop point of grease. The polytetrafluoroethylene (PTFE) and lithium complex thickeners show the highest drop point among various thickeners, and their maximum working temperature range up to 177 ^{o}C.

3.5.2 Thermogravimetric analysis (TGA) of greases

Thermogravimetric analysis is used to assess the decomposition of materials by observing the variation in mass with temperature. It is a quantitative measurement technique that helps to estimate moisture, volatile, and filler contents in the samples. The weight loss of grease as a function of temperature was recorded using a thermogravimetric analyzer (TGA, Diamond, PerkinElmer) in a temperature range between 45 and 700 °C under the environment of nitrogen at a heating rate of 10 °C min^{-1}.

3.5.3 Microstructural study of greases

The microstructural images of paraffin–based lithium grease samples were studied using a scanning electron microscope (SEM; Zeiss EVO 18 Research, Oberkochen, Germany). The oil content of grease samples was extracted before microscopic studies. In this context, a skinny layer of grease sample was spread over a glass slide. The thin film of the grease sample on the glass slide was immersed in n–hexane for 15–20 min to remove the base oil content, and then the specimen was baked in a hot air oven at 65–70 °C. It was followed by a gold coating on a dried thin film of grease for capturing microscopic images. Each

sample of grease was prepared following a similar protocol for microscopic evaluation. The typical accelerating voltage was kept constant at 20 kV, and the working distance between the electron gun and specimen was maintained in the range between 10–10.5 mm.

3.5.4 Rheological study of greases

The rheological properties of grease samples were carried out using Anton Parr rheometer (Model: MCR102; plate–plate geometry; diameter of each plate: 50 mm; the gap between plates: 1 mm). The viscous flow test was done within the linear viscoelastic range in a shear rate range of 0–100 s^{-1}. The small–amplitude oscillatory shear (SAOS) test was performed between 0–100 $rad.s^{-1}$. The viscous flow and SAOS tests were executed at 75 °C. Each test was repeated for the consistency of the results. The experimentally acquired shear stress vs strain curves was fitted with the Herschel–Bulkley model and comprised three characteristics rheological parameters; yield stress (τ_y), consistency factor (k), and shear–thinning index (n) as per the following equation:

$$\tau = \tau_y + k\dot{\gamma}^n \qquad \text{Eq (3.4)}$$

Further, the apparent viscosity of grease was computed as follows:

$$\eta = \frac{\tau}{\dot{\gamma}} \qquad \text{Eq (3.5)}$$

Where η, τ, and $\dot{\gamma}$ represent apparent viscosity, shear stress, and shear rate, respectively.

3.5.5 Characterization of tribological properties of grease using four–ball tester

The four–ball tester was manufactured by DUCOM Instruments Pvt. Ltd., India (model: TR–30H–KRL–RFA). The schematic diagram of the four–ball tester is shown in **Figure 3.11**. It was used to assess the AW and EP properties of grease samples as per ASTM D2266 and ASTM D2596 standards, respectively. Four identical 12.7 mm or ½ inch

diameter chrome steel (SKF) balls were used as specimens. The specifications of specimen and test conditions used to evaluate of AW and EP properties of the grease are summarized in **Table 3.5**.

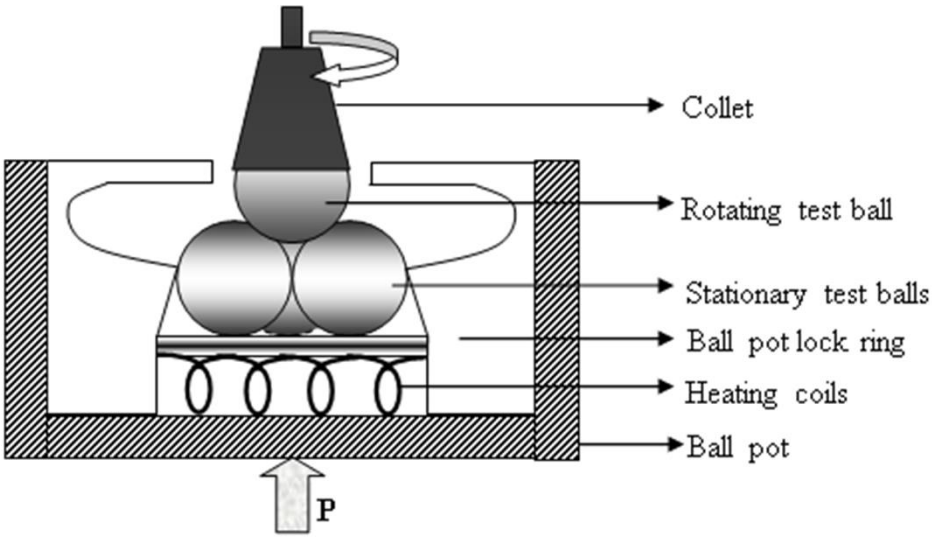

Figure 3.11: Schematic diagram of four–ball tester

Table 3.5: The details of specimens and test conditions used in four–ball tester

Test specifications	AW test	EP Test
Specimens	Material – AISI–52100 Dia. (ϕ) = 12.7 mm Hardness – 59–61 HRC Young's modulus – 210 GPa Poisson's ratio – 0.3 Roughness (S_q) – 0.201 µm	Material – AISI–52100 Dia. (ϕ) = 12.7 mm Hardness – 59–61 HRC Young's modulus – 210 GPa Poisson's ratio – 0.3 Roughness (S_q) – 0.201 µm
Standard	ASTM D2266	ASTM D2596
Speed, rpm	1200 ± 60	1760±40
Temperature, ^oC	75±2	27±8
Load, kgf	40±0.2	6, 8, 10,13, 16, 20, 24, 32, 40, 50, 63, 80, 100, 126, 160, 200, 250, 315, 400, 500, 620, 800
Duration, s	3600±60	10

New steel balls were used in each test experiment. The steel balls, ball chuck, and ball pot were thoroughly cleaned in acetone for ten min to remove the dirt and oil contaminations with the aid of an ultrasonic bath before the tribological tests. The three steel balls were clamped in the ball pot, and the top ball as a counter body was rotated over the three stationary balls under the applied load. The ball pot was filled with the grease sample. The load was applied using a lever mechanism. As per ASTM D2266, the AW test duration was 60 min. The friction values were recorded throughout the test via a computer with software interfaced with the four–ball tester. The average COF was calculated by considering all the data points. The ball and ball tribo–pair formed a non–conformal contact. The maximum contact pressure (P_{max}) developed between the contact point was found to be 3.4 GPa, and the detailed calculations of P_{max} are presented in **Appendix–B**. The diameter of worn scars developed on three stationary balls during each test was measured by image acquisition. Further, the detailed calculations of the wear volume of steel balls are presented in **Appendix–C**. The EP test was conducted to determine the last non–seizure and weld loads. This test was conducted with various loads for 10 s until the steel balls were welded together due to frictional heat. Each AW and EP test was repeated thrice and reported the average value of these results.

The minimum film thickness (h_{min}) developed by different grease samples between tribo–pairs and the film thickness parameter (λ) were computed considering the hard elastohydrodynamic lubrication (EHL) regime. The h_{min} is dependent on the geometrical and mechanical properties of the test balls, test conditions, and physicochemical properties of the base oil used in the grease formulation. The mechanical and geometrical properties and test conditions are listed in **Table 3.5**. The h_{min} developed by paraffin grease, castor grease, and coconut grease between tribo–pairs were estimated to 46 nm, 115 nm, and 21 nm, respectively. In the estimation of h_{min}, the role of thickener was not considered. The

detailed calculations of h_{min} and λ are presented in **Appendix–D**. The $\lambda < 1$ for all base oils signifies that tribo–pairs were operating under the boundary lubrication regime. Further, the detailed calculations of energy consumption due to friction are presented in **Appendix–E**.

3.5.6 Characterization of tribological properties of grease using SRV–5 machine

High–frequency linear–oscillation (SRV–5 model) test machine was used to evaluate the tribological properties of grease samples as per the ASTM D5707 standard. The schematic representation of the SRV–5 test machine is depicted in **Figure 3.12**. A chrome steel ball oscillated under constant load against a chrome steel disc. The steel ball and disc were cleaned thoroughly using acetone and hexane to remove the dirt and oil contaminants. The specifications of specimen and test conditions used to evaluate AW properties of the greases are summarized in **Table 3.6**.

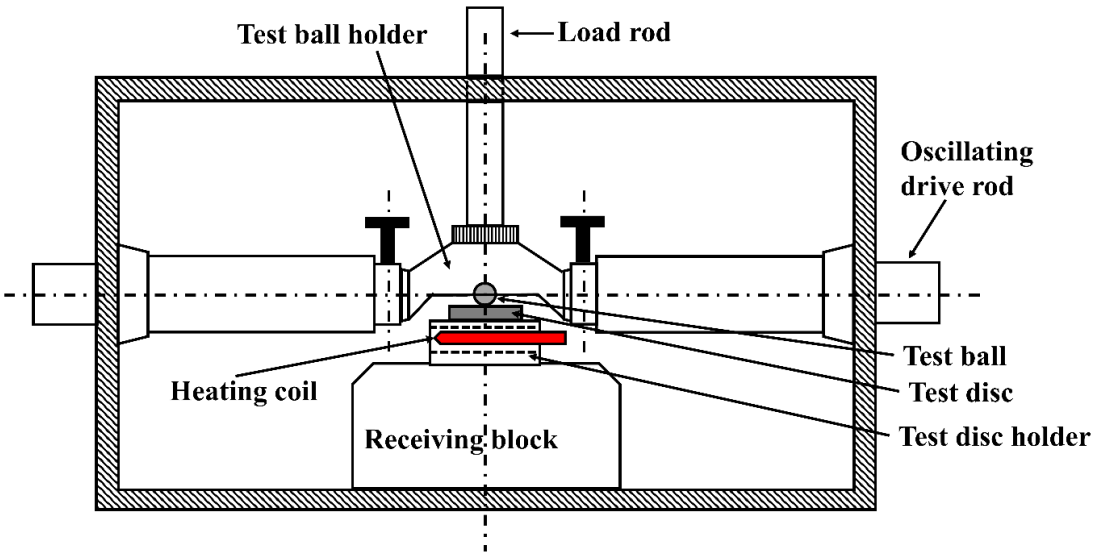

Figure 3.12: Schematic diagram of the SRV test machine

Table 3.6: The details of specimens and test conditions used in SRV–5machine

Test specifications	AW test
Specimens	Ball (ϕ) = 10 mm, Disc = 24×7.85 mm Material – 100Cr6 Hardness – 60±2 HRC Young's modulus – 210 GPa Poisson's ratio – 0.3 Roughness (S_q) – 0.20 µm
Standard	ASTM D5707
Load, N	50 N for 30 s (pre–load), then 200 N
Stroke amplitude, mm	1.0
Temperature, ^oC	80
Duration, min	120±0.25

0.1 g to 0.2 g lubricating grease was placed on the steel disc. The grease sample was placed between the ball and the disc. The load was applied on the tribo–pairs and subjected to high–frequency linear oscillation motion under prescribed test conditions. The friction values were recorded throughout the test via computer software interfaced with the SRV test machine. The average COF was calculated by considering all the data points. The disc and ball tribo–pair formed a non–conformal contact. The maximum contact pressure (P_{max}) was found to be 2.74 GPa, and the detailed calculations of P_{max} are presented in **Appendix–B**. The planimetric wear (W_q) of the disc was acquired across the wear track via profilometric measurements (Hommeltester, Fa. Hommel, Hanau, Germany). After the test, the radius of the steel ball (R') was measured by a profilometer and estimated the wear volume (W_V) of the ball and disc. Further, the detailed calculations for estimating the wear volume of steel ball and disc are presented in **Appendix–C**.

3.6 Characterization of worn surfaces

3.6.1 Scanning electron microscope (SEM) and Energy–dispersive X–ray spectroscopy (EDS)

The microstructural features of grease and worn surfaces of test samples were examined in a scanning electron microscope (SEM), Zeiss EVO 18 Research, Oberkochen, Germany. After the tribo–test, the specimens were cleaned with acetone to remove traces of grease. The typical accelerating voltage was kept constant at 20 kV, and the working distance between the electron gun and specimen was maintained in the range between 10–10.5 mm. The elemental composition of worn surfaces was analyzed using energy–dispersive X–ray spectroscopy (EDS) integrated with the SEM.

3.6.2 X–ray photoelectron spectroscopy (XPS)

XPS, a quantitative spectroscopic technique is used to probe the chemical composition of specimens. The X–ray photoelectrons are characteristic electrons ejected from the uppermost atomic layer of specimens when an atom absorbs an X–ray photon. The electron emitted from the electron shell of an atom exhibits characteristics energy levels, unveiling the composition of chemical elements in the sample being examined. Therefore, the XPS technique is referred to as a surface chemical analysis. The XPS operates under ultra–high vacuum (10^{-9} bar). The chemical composition of the tribo–film developed on the worn surface was examined by XPS (Thermoscientific, K–Alpha) using Al Kα radiation X–ray source. The binding energies of all spectra were calibrated with the C 1s and binding energy of 284.5 eV.

3.6.3 Scanning probe microscope (SPM)

The three–dimensional morphology of worn surfaces of steel balls was scanned using a scanning probe microscope (SPM), NTEGRA Prima, NT–MDT Spectrum Instruments, Russia. Primarily, the worn surface was cleaned with acetone, and the roughness of the worn area of 20×20 µm and 50×50 µm was measured with a silicon nitride cantilever (tip radius:10 nm) in a tapping mode at a scanning rate of 0.5 Hz. The 15 nN contact force was applied to avoid any surface damage when the probe was crossing the worn area. The resolution of all captured images was 768×768 pixel.

3.7 Summary of the chapter

This chapter provides an overview of the approaches used for synthesizing nanoadditives, greases, tribo–testing, and methods used to calculate the tribological parameters. Further, the chapter describes a brief introduction of all analytical tools used in this thesis work.